Low-Frequency Signals in Long Tree-Ring Chronologies for Reconstructing Past Temperature Variability

Jan Esper,[1] Edward R. Cook,[2]* Fritz H. Schweingruber[1]

Preserving multicentennial climate variability in long tree-ring records is critically important for reconstructing the full range of temperature variability over the past 1000 years. This allows the putative "Medieval Warm Period" (MWP) to be described and to be compared with 20th-century warming in modeling and attribution studies. We demonstrate that carefully selected tree-ring chronologies from 14 sites in the Northern Hemisphere (NH) extratropics can preserve such coherent large-scale, multicentennial temperature trends if proper methods of analysis are used. In addition, we show that the average of these chronologies supports the large-scale occurrence of the MWP over the NH extratropics.

Much of the current debate on the Earth's climate variability is driven by the observation of a modern, century-long temperature increase, culminating with the last decade of the 20th century as the warmest since 1856 (*1*). These dramatic recent temperature changes have been related to those of the last millennium by the Mann-Bradley-Hughes (MBH) multiproxy reconstruction of NH annual temperatures (*2*). By combining instrumental temperature data with long, temperature-sensitive proxy records, the MBH reconstruction indicates that the 20th-century warming is abrupt and truly exceptional. It shows an almost linear temperature decrease from the year 1000 to the late 19th century, followed by a dramatic and unprecedented temperature increase to the present time. The magnitude of warmth indicated in the MBH reconstruction for the MWP, ~1000–1300 (*3*, *4*), is uniformly less than that for most of the 20th century.

The MBH reconstruction has been criticized (*5*) for its lack of a clear MWP. Critics argue that tree-ring records, the substantial basis of the MBH reconstruction before the 17th century, cannot preserve long-term, multicentennial temperature trends. This contention is of fundamental importance because if tree-ring reconstructions are limited in this way, then including such records in hemispheric estimates of past temperatures would bias the results as argued (*5*). To illustrate that this need not be the case, we present the analysis of centuries-long ring-width trends in 1205 radial tree-ring series from 14 high-elevation and middle-to-high latitude sites distributed over a large part of the NH extratropics (Fig. 1). Tree species represented in this collection are from the genera *Picea*, *Pinus*, *Larix*, and *Abies*. Using these data, we demonstrate that multicentennial temperature information can be preserved in long tree-ring records provided that the data are properly processed to preserve such low-frequency information due to climate. We also show that the MWP was likely to have been a large-scale phenomenon in the NH extratropics that appears to have approached, during certain intervals, the magnitude of 20th-century warming, at least up to 1990.

Most millennia-long tree-ring chronologies are averages of many tree-ring series from living and dead trees. The segment lengths of these series are typically 200 to 400 years long, and the overlapping individual series are exactly aligned by calendar year and connected in time using a method known as "cross-dating" (*6*). The difficulty of preserving multicentennial variation in such tree-ring series, when the segment lengths are substantially shorter than the length of the overall chronology being developed, results from the removal of age-related biological growth trends that represent noise for the purpose of climatic reconstruction (*6*). These growth trends occur almost universally in "raw" tree-ring measurement series and frequently describe a downward trend of ring width with increasing age. Dendrochronologists usually eliminate these growth trends by detrending each tree-ring width series with a fitted smooth mathematical growth function. In such cases, the maximum wavelength of recoverable climatic information is fundamentally limited by the segment lengths of the individual detrended series (*7*). Thus, a 100-year-long tree-ring series will not contain any climatic variance at periods longer then 100 years if it is explicitly detrended by a fitted growth curve. Consequently, the problem of missing long-term trends in millennia-length tree-ring chronologies is due to using detrended series that are short relative to the multicentennial fluctuations due to climate (*8*). Exceptions are chronologies built with 1000 year or longer individual tree-ring series (*9*, *10*) and chronologies developed by Regional Curve Standardization (RCS) (*11*) or Age Banding (*12*) methods.

Several of the tree-ring collections analyzed here have been described and used previously in individual and large-scale temperature reconstructions and related studies (*11*, *13*–*19*). Ring widths of trees growing in cold environments usually reflect the influence of warm-season temperatures on growth most strongly. However, in some cases, they also reflect temperatures from the cool-season months before the radial growth season as well (*20*). Here, we will not explicitly model the temperature signals of the individual tree-ring chronologies, because this has mostly been done already (*11*, *13*–*19*). Rather, we will demonstrate the preservation of coherent multicentennial variability among the 14 tree-ring sites, which is inferred to reflect large-scale, multicentennial temperature changes over the past 1000 years in the NH extratropics. These inferred changes are almost certainly weighted toward the warm-season months, as some previous studies have shown (*11*, *13*, *18*, *19*). Even so, low-frequency warm-season and annual temperature trends recorded in NH instrumental data are statistically indistinguishable (*8*).

To preserve possible multicentennial growth trends due to climate, we analyzed the individual raw ring-width measurements using

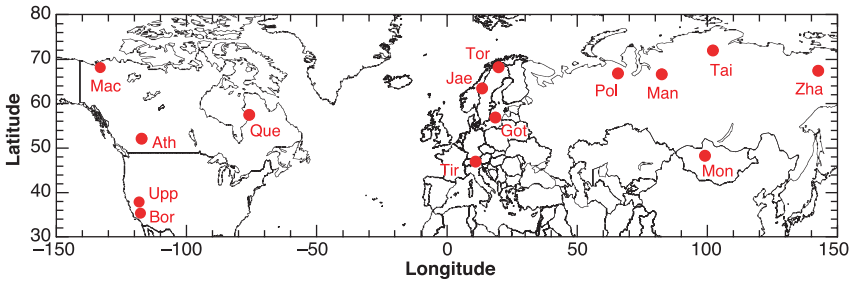

Fig. 1. Map of the 14 tree ring sampling sites. Ath, Athabasca; Bor, Boreal; Mac, Mackenzie; Que, Quebec; Upp, Upperwright; Got, Gotland; Jae, Jaemtland; Tir, Tirol; Tor, Tornetraesk; Man, Mangazeja; Mon, Mongolia; Pol, Polar Urals; Tai, Taimir; and Zha, Zhaschiviersk.

[1]Swiss Federal Research Institute WSL, Zuercherstrasse 111, 8903 Birmensdorf, Switzerland. [2]Lamont-Doherty Earth Observatory, Palisades, NY 10964, USA.

*To whom correspondence should be addressed. E-mail: drdendro@ldeo.columbia.edu

RCS, a method that has been used previously for reconstructing long-term temperature variability from tree rings (*11*). Successful use of the RCS method generally requires a large number of ring-width series because the method of detrending is not based on any explicit curve-fitting to the individual series as described above. Rather, a single mean biological growth curve, estimated from all the data, is used (*8*). Consequently, systematic departures of actual growth of individual series from the regional curve (RC) are common. Indeed, this is why the RCS method can preserve trends in excess of the lengths of the individual records being detrended (*7*, *11*). When systematic departures from the RC occur commonly among series in a given time period, this may reflect a low-frequency change in climate forcing on growth.

To build RCS chronologies from the whole data set that contains different sites and species, we analyzed the growth levels and trends of the individual ring-width series after aligning them by cambial age and classifying them into two groups: one with age trends that have a weakly "linear" form (443 series) and one with age trends that are more "nonlinear" (762 series) (*8*). The data sets were divided this way because differences in growth levels and slopes can bias resulting RCS chronologies (*21*). For example, according to their mean age trends (*8*), the young nonlinear trees grow 2 to 3 times faster than the linear trees up until 200 years of age.

Two smoothed RCs were estimated from the averaged biological age-aligned data in the linear and nonlinear groups. Tree-ring departures from each RC were calculated as ratios for the linear and nonlinear data sets following standard procedures (*6*). The resulting tree-ring indices were then averaged into linear and nonlinear mean value functions to produce two nearly independent tree-ring chronologies covering the years 800–1990 (Fig. 2A). For each chronology, the changes in sample size each year are indicated in Fig. 2B, with a more detailed description of changing individual site contributions provided in (*8*). The two chronologies are very similar over the past ~1200 years. Each shows evidence for inferred above-average temperatures during the MWP (900–1300), although some differences in the timing of peak conditions are evident. This may reflect weakness of sample depth before the year 1200 (Fig. 2B), and the lack of uniform spatial representation as the number of sites decreases back in time (*8*). However, it could also reflect higher spatial variability of MWP temperatures in the NH extratropics (*22*). More tree-ring collections that span the MWP are needed that are long and well-replicated to determine which hypothesis is correct.

After the year 1200, the linear and nonlinear RCS chronologies lock together remarkably well at multidecadal and centennial time scales. There is strong evidence for inferred below-average temperatures over much of the 1200–1850 interval, which may be regarded as a NH extratropical expression of the Little Ice Age (LIA) (*23*). Since the year 1850, large-scale warming in the NH extratropics is indicated, in agreement with instrumental temperature records (*1*). Overall, the broad coherency and rich multicentennial variability found in the linear and nonlinear chronologies demonstrate that properly selected and processed tree-ring records can preserve such long time-scale climate variability. This result refutes the contention (*5*) that long-term tree-ring records can not preserve multicentennial fluctuations due to climate.

We also provide a combined analysis of the linear and nonlinear RCS-detrended data sets, with two-tailed 95% bootstrap confidence intervals (*8*). In this case, the mean value function and its confidence intervals (Fig. 2C) have been rescaled to reflect changes in absolute radial increment (mm) due to climate. This provides some idea about long-term changes in carbon sequestration in the stems of these temperature-sensitive trees. Figure 2C identifies periods of growth that depart significantly ($P < 0.05$) from the long-term mean. These intervals include episodes in the MWP, LIA, and the 20th century. The conspicuous increase in the confidence limits after 1950 may also reflect the anomalous reduction in growth performance found at some high northern latitude conifer sites (*24*). Regardless, the confidence limits provide compelling evidence that the low-frequency growth variations obtained from these 14 tree-ring sites are real and are probably due to large-scale temperature variations over the NH extratropics.

Even though the true RCS temperature signal is undoubtedly weighted toward the warm-season months, we can usefully calibrate it as an annual temperature record for comparison to MBH because of the very high correlation (r = 0.94) between NH annual and warm-season temperatures (*8*). Correlations between the mean RCS chronology and NH (0° to 90°N) mean annual instrumental temperatures (Table 1) over the 1856–1980 period indicate the presence of a temperature

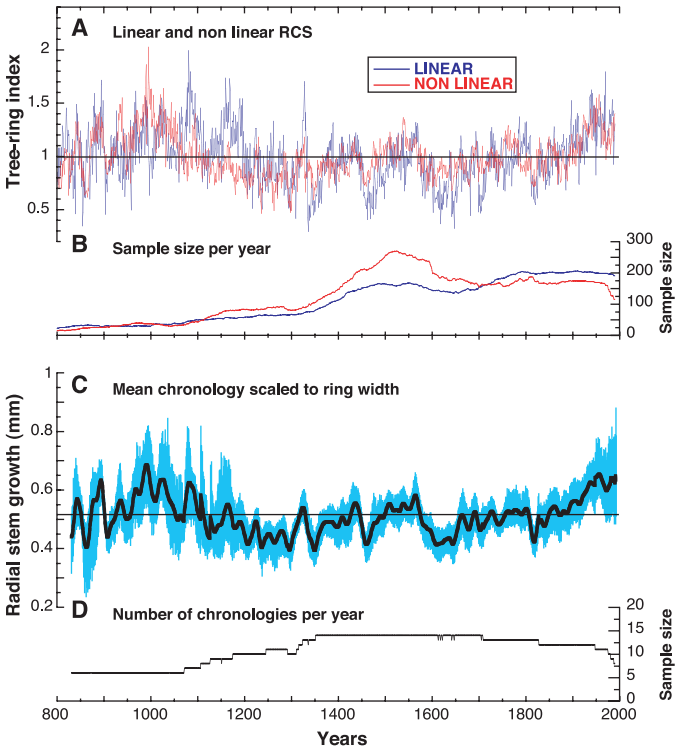

Fig. 2. RCS chronologies of linear and nonlinear classified trees (**A**), the yearly sample size for each chronology (**B**), the 20-year smoothed NH extratropics reconstruction of radial stem productivity in high elevation and high latitude forest environments since ~800 (black) and two-tailed 95% bootstrap confidence intervals (blue) (**C**), and the number of chronologies available for the reconstruction each year (**D**). The NH reconstruction was derived from the 14 site RCS chronologies after each was smoothed with a 20-year low-pass filter to emphasize multidecadal to multicentennial time scales. The two-tailed 95% confidence limits were estimated with the use of a bootstrap procedure (*8*).

Table 1. Correlations between instrumental mean annual temperatures (0° to 90°N) and the MBH reconstruction and mean RCS tree-ring chronology before and after digital filtering. The filtered series are 40-year low-pass (MBH series ends in 1977), 20-year low-pass, and 20-year high-pass. The time period is 1856–1980. Orig., unfiltered data; LP, low-pass; HP, high-pass.

Series	Orig.	40-year LP	20-year LP	20-year HP
MBH	0.82	0.96	0.95	0.59
RCS	0.59	0.88	0.84	0.15

signal in the tree rings at interdecadal and longer time scales (40-year low-pass, 20-year low-pass), but not for interannual to decadal variability (20-year high-pass). The low-pass RCS correlations also compare favorably with those for the MBH reconstruction (Table 1). In contrast, the RCS 20-year high-pass correlation is noticeably weaker than that of MBH. However, MBH contains some long-term instrumental measurements (*2*), which undoubtedly improves its relation with NH instrumental temperatures at all frequencies.

Figure 3 shows the mean RCS chronology, rescaled now to estimates of NH annual temperature (to be compatible with MBH) and the MBH temperature reconstruction itself (*8*), each with 95% confidence limits. Each series has been smoothed with a 40-year low-pass filter to emphasize the multidecadal to multicentennial changes in temperature. The 40-year low-pass filtered mean RCS chronology was scaled to NH annual temperatures using 1900–1977 as the calibration period. This time period was chosen because it represents the interval most similar between RCS and MBH ($r = 0.94$). For comparison, the correlations of RCS and MBH with 40-year low-pass NH (0° to 90°) annual temperatures are 0.98 and 0.97, respectively. These very high correlations are because the filtered data have similar trends in the 20th century.

When the mean RCS chronology is expressed this way, striking differences in low-frequency behavior with MBH are revealed. This comparison suggests that MBH is not necessarily missing a MWP. Rather, it has a reduced expression of the LIA compared with RCS. Correlations between RCS and MBH (Table 2) indicate that this disagreement is largely confined to periods longer than 200 years. At shorter periods, the RCS and MBH series are almost synchronous. These results are consistent with comparisons of MBH to other long proxy temperature reconstructions (*25*).

We have demonstrated how multicentennial temperature variability in long tree-ring records can be preserved if the appropriate tree-ring data and proper methods of analysis are used. This result is not new (*11*, *13*, *18*), but the way it has been demonstrated is somewhat novel and instructive. In so doing, evidence for a large-scale MWP (sensu lato) has been reconstructed, and it approaches the magnitude of 20th-century warming in the NH up to 1990. Consistent with other analyses of the MWP (*4*, *22*) and with our comparisons of the linear and nonlinear RCS chronologies (Fig. 2A), the MWP appears to be more temporally variable than the warming trend of the last century. Our analysis also indicates that the MWP in NH extratropics may have begun in the early 900s (Fig. 2C). The warmest period covers the interval 950–1045, with the peak occurring around 990, a result consistent with another analysis using some of the same tree-ring data (*18*). This finding suggests that past comparisons of the MWP with the 20th-century warming back to the year 1000 (*19*, *22*) have not included all of the MWP and, perhaps, not even its warmest interval.

The good agreement between the RCS and MBH records at all time scales except multicentennial is remarkable, given that the mean RCS chronology is simply a large-scale average of uncalibrated tree-ring data. MBH has two data sets in common with RCS (Tornetraesk and Polar Urals) that are largely restricted to the nonlinear group (*8*). Yet the linear and nonlinear RCS chronologies are extremely similar (Fig. 2A). Thus, the noted similarities between RCS and MBH are unlikely to be due to the small amount of data overlap between the series.

Where the two series disagree is on multicentennial time scales, which relates to the criticism noted earlier (*5*). The MBH reconstruction includes temperature estimates from the tropical and subtropical NH (*2*), which is not represented in the RCS record. This may explain some of the observed differences. Much of the multicentennial variability in MBH has also been replicated by an energy balance model that includes solar, volcanic aerosol, anthropogenic aerosol, and greenhouse gas forcing (*26*). Therefore, the large multicentennial differences between RCS and MBH are real and would seem to require a NH extratropical forcing to explain them, one that attenuates toward the equator. One candidate is the 1000- to 2000-year climate rhythm (1470 ± 500 years) in the North Atlantic, which may be related to solar-forced changes in thermohaline circulation (*27*, *28*). The degree to which this mode of climate forcing is responsible for the multicentennial variations in RCS requires further investigation.

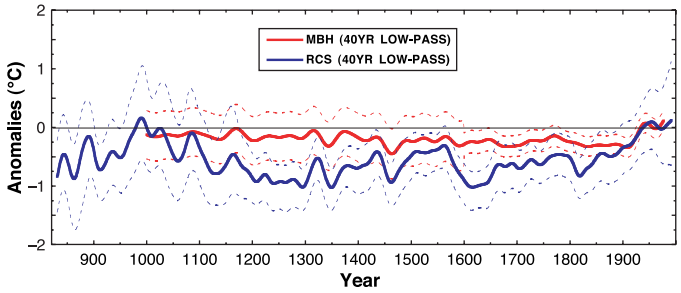

Fig. 3. Comparison of the MBH NH temperature reconstruction with the mean RCS chronology scaled to the MBH record using the 1900–1977 period for calibration. The RCS confidence intervals are estimated using the bootstrap method (*8*). Each series (solid lines) and its confidence intervals (dashed lines) have been smoothed with 40-year low-pass filters to emphasize the multidecadal to multicentennial time scales. The filtered MBH data was kindly supplied by M. E. Mann. Correlations between unfiltered and filtered versions of these records (Table 2) show that the mean RCS chronology is well related to the MBH reconstruction at multidecadal to centennial time scales. However, the two disagree at multicentennial time scales.

Table 2. Correlations between the mean RCS chronology and the MBH temperature reconstruction over two time periods and for different bandwidths of variability. The first interval truncates the periods associated with the MWP and 20th-century warming where the greatest differences between the records are evident. The second time period covers the full overlap of the two records. Only when the multicentennial fluctuations (200 YR LP) are correlated do we see a lack of agreement. BP, band-pass.

Interval	Orig.	200-year LP	200-year HP	20- to 200-year BP	20-year HP
1100–1850	0.30	−0.37	0.47	0.68	0.24
1000–1980	0.40	0.43 (0.09*)	0.41	0.60	0.24

*Correlation minus the 1851–1980 data.

References and Notes

1. P. D. Jones, M. New, D. E. Parker, S. Martin, I. G. Rigor, *Rev. Geophys.* **37**, 173 (1999).
2. M. E. Mann, R. S. Bradley, M. K. Hughes, *Geophys. Res. Let.* **26**, 759 (1999).
3. H. H. Lamb, *Palaeogeogr. Palaeoclim. Palaeoecol.* **1**, 13 (1965)
4. M. K. Hughes, H. F. Diaz, *Clim. Change* **26**, 109 (1994).
5. W. S. Broecker, *Science* **291**, 1497 (2001).
6. E. R. Cook, L. A. Kairiukstis, Eds., *Methods of Dendrochronology* (Kluwer Academic Publishers, Dordrecht, Netherlands, 1990).
7. E. R. Cook, K. R. Briffa, D. M. Meko, D. A. Graybill, G. Funkhouser, *The Holocene* **5**, 229 (1995).
8. Supplementary details are available on *Science* Online at www.sciencemag.org/cgi/content/full/295/5563/2250/DC1.
9. V. C. LaMarche, *Science* **183**, 1043 (1974).
10. J. Esper, F. H. Schweingruber, M. Winiger, *The Holocene* **12**, 267 (2002).
11. K. R. Briffa *et al.*, *Clim. Dyn.* **7**, 111 (1992).
12. K. R. Briffa *et al.*, *J. Geophys. Res.* **106**, 2929 (2001).
13. K. R. Briffa, P. D. Jones, F. H. Schweingruber, S. G. Shiyatov, E. R. Cook, *Nature* **376**, 156 (1995).
14. B. H. Luckman, K. R. Briffa, P. D. Jones, F. H. Schweingruber, *The Holocene* **7**, 375 (1997).
15. A. H. Lloyd, L. J. Graumlich, *Ecology* **78**, 1199 (1997).
16. R. D'Arrigo *et al.*, *Geophys. Res. Lett.* **28**, 543 (2001).
17. J. M. Szeicz, G. M. MacDonald, *Quat. Res.* **44**, 257 (1995).
18. K. R. Briffa, *Quat. Sci. Rev.* **19**, 87 (2000).
19. P. D. Jones, K. R. Briffa, T. P. Barnett, S. F. B. Tett, *The Holocene* **8**, 477 (1998).
20. G. C. Jacoby, R. D. D'Arrigo, T. Davaajamts, *Science* **273**, 771 (1996).
21. J. Esper, E. R. Cook, K. Peters, *Tree-Ring Res.*, in press.
22. T. J. Crowley, T. S. Lowery, *Ambio* **29**, 51 (2000).

23. J. M. Grove, *The Little Ice Age* (Methuen, London, 1987).
24. K. R. Briffa *et al.*, *Nature* **391**, 678 (1998).
25. P. D. Jones, T. J. Osborn, K. R. Briffa, *Science* **292**, 662 (2001).
26. T. J. Crowley, *Science* **289**, 270 (2000).
27. G. Bond *et al.*, *Science* **278**, 1257 (1997).
28. G. Bond *et al.*, *Science* **294**, 2130 (2001).
29. We gratefully acknowledge B. Luckman (Athabasca), L. Graumlich and A. Lloyd (Boreal and Upperwright), J. Szeicz (Mackenzie), S. Payette and L. Filion (Quebec), T. Bartholin and W. Karlén (Gotland, Jaemtland, Torne-traesk), V. Siebenlist-Kerner (Tirol), S. Shiyatov (Polar Urals, Mangazeja), G. Jacoby (Mongolia), M. Naurzbaev (Taimir), and F. Schweingruber (Zhaschiviersk), who sampled the tree-ring data sets in 14 different regions of the Northern Hemisphere and/or made them available to this study. We also appreciate the discussions with K. Briffa, P. Jones, and T. Osborn on error estimation and thank other colleagues for vigorous discussions on various aspects of this paper. This work was supported by the Max Kade Foundation, Inc., during a research visit at the Lamont-Doherty Earth Observatory of Columbia University in New York (J.E.). Lamont-Doherty Earth Observatory Contribution No. 6301.

12 September 2001; accepted 11 February 2002

Coda Wave Interferometry for Estimating Nonlinear Behavior in Seismic Velocity

Roel Snieder, Alexandre Grêt, Huub Douma, John Scales

In coda wave interferometry, one records multiply scattered waves at a limited number of receivers to infer changes in the medium over time. With this technique, we have determined the nonlinear dependence of the seismic velocity in granite on temperature and the associated acoustic emissions. This technique can be used in warning mode, to detect the presence of temporal changes in the medium, or in diagnostic mode, where the temporal change in the medium is quantified.

In many applications, such as nondestructive testing or monitoring of volcanoes or radioactive waste disposal sites, one is primarily interested in detecting temporal changes in the structure of the medium. Temporal changes in Earth's structure that accompany earthquakes have been observed on the basis of the attenuation of coda waves (*1*), on the arrival times of the directly arriving waves (*2*), on velocity changes inferred from later arriving waves (*3*) [see also (*4*)], and on changes in seismic anisotropy (*5*). Here, we introduce coda wave interferometry whereby multiply scattered waves are used to detect temporal changes in a medium by using the scattering medium as an interferometer. For quasi-random perturbations of the positions of point scatterers, or for a change in the source location or the wave velocity, estimates of this perturbation can be derived from multiply scattered waves by a cross correlation in the time domain.

In the numerical example (Fig. 1), the wave field for a medium consisting of isotropic point scatterers is computed with the use of a deterministic variant (*6*, *7*) of Foldy's method (*8*). Given the mean free path (l = 20.1 m) and the wave velocity (v = 1500 m/s), one can infer that after $t = 5.4 \times 10^{-2}$ s the waves are on average scattered more than three times. The later part of the signal is called the coda. Suppose that one repeats this multiple scattering experiment after the scatterer locations are perturbed. The perturbation in the scatterer location is 1/30 of the dominant wavelength and is uncorrelated between scatterers (*9*).

In this example, the scatterers' locations are perturbed. In general, a perturbation can involve other changes in the medium or a change in source location. We refer to the waveform before the perturbation as the unperturbed signal and to the waveform after the perturbation as the perturbed signal. For early times ($t < 0.04$ s), the waves in Fig. 1 have not scattered often, rendering the path lengths of these waves insensitive to the small perturbations of the scatterers (small compared with the dominant wavelength $\lambda = 2.5$ m), which causes the unperturbed and perturbed signals to be similar. However, the multiply scattered waves are increasingly sensitive with time to the perturbations of the scatterer locations because the waves bounce more often among scatterers as time increases. The correlation between the unperturbed and perturbed signals, therefore, decreases with increasing time.

The perturbation in the medium can be retrieved from the cross correlation of the coda waves recorded before and after the perturbation. The unperturbed wave field $u_{\mathrm{unp}}(t)$ can be written as a Feynman path summation (*10*) over all possible paths P

$$u_{\mathrm{unp}}(t) = \sum_P A_P S(t - t_P), \qquad (1)$$

where a path is defined as a sequence of scatterers that is encountered, t_P is the travel time along path P, A_P is the corresponding amplitude, and $S(t)$ is the source wavelet. When the perturbation of the scatterer locations (or source location) is much smaller than the mean free path, the effect of this perturbation on the geometrical spreading and the scattering strength can be ignored, and the dominant effect on the waveform arises from the change in the travel time τ_P of the wave that travels along each path

$$u_{\mathrm{per}}(t) = \sum_P A_P S(t - t_P - T_P). \qquad (2)$$

The time-windowed correlation coefficient is computed from

$$R^{(t,T)}(t_s) \equiv \frac{\int_{t-T}^{t+T} u_{\mathrm{unp}}(t')u_{\mathrm{per}}(t'+t_s)dt'}{\left(\int_{t-T}^{t+T} u^2_{\mathrm{unp}}(t')dt' \int_{t-T}^{t+T} u^2_{\mathrm{per}}(t')dt'\right)^{1/2}} \qquad (3)$$

where the time window is centered at time t with duration $2T$ and t_s is the time shift used in the cross correlation. When Eqs. 1 and 2 are inserted, double sums $\Sigma_{PP'}$ over all paths appear. In

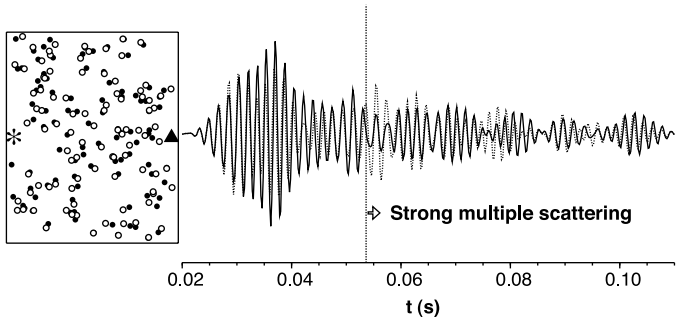

Fig. 1. Location of 100 scatterers before and after the perturbation (filled circles and open circles, respectively) with the source (asterisk) and receiver location (triangle). For the sake of clarity, the scatterer displacement is exaggerated by a factor 40. The scatterers are placed in an area of 40 m by 80 m. The waveforms recorded before and after the perturbation at the receiver are shown on the right with a solid and dashed line, respectively.

Department of Geophysics and Center for Wave Phenomena, Colorado School of Mines, Golden, CO 80401, USA.